The Effect of Location on the Structure and Mechanical Properties of Selective Laser Melted 316L Stainless Steel

E. Fitzgerald[1]*, W. Everhart[1]

[1] National Security Campus, Kansas City, MO 64147

Abstract

Additive Manufacturing (AM) has significantly increased the design freedom available for metal parts and provides flexibility within each build to produce multiple components of varying size and shape. In order to obtain the highest build efficiency, it is ideal to print multiple parts together spanning the entire plate, with as little spacing as possible between the parts. Work has been performed to characterize the variance of materials properties as a function of location within the build volume. This work utilizes mechanical, chemical, and structural analysis techniques to expand on previous work by statistically evaluating the impact of build location on tensile performance in Selective Laser Melting (SLM). Results show that properties span a small range regardless of build design. Specific effects of cover gas convection, location, and build length are observed and evaluated. Finally, sub-grain misorientation values are correlated to material strength through Electron Back Scatter Diffraction (EBSD).

Introduction

The adoption of metal additive manufacturing (AM) has grown over the past decade due in no small part to the newly available geometric freedom and the capability to customize each build based on the number and size of any variety of components. As these new technologies are adapted and used to manufacture goods on larger scales, it is important to understand the variables in the machine and the impact those variables have on the built material. Many studies have investigated the effect of scanning parameters on residual stress, bulk properties and microstructure in AM [1-12]. These studies include evaluation of the structure, residual stresses, and properties generated by the fast cooling rates present in AM. Secondary build variables, used here to describe variables outside of machine scanning parameters like location or orientation of a part in the build, proximity of neighboring parts and machine operations, may affect local temperature gradients but are commonly assumed to be insignificant.

Electron Beam Melting (EBM) is an example of a technology wherein several studies have included information on the impact of secondary build variables on material microstructure and performance [1-4]. N. Hrabe and T. Quinn [1, 2] investigated the location of the part in the build and found no significant effect on the microstructure and material properties. They did observe a small statistical difference in yield and tensile strength by part size, but could not determine a relationship between strength and size of the part. In the study samples of each size were printed

as a group in different regions of the build chamber, therefore location may play a role, not just size. Additional research into the microstructure throughout the height in a EBM build has shown there was no effect on material density but variability in microstructure can be seen [3,4]. This change in microstructure corresponded to a reduction in material strength and hardness.

As for Selective Laser Melting (SLM) technology, secondary build variables have been less investigated. Abd-Elghany and Bourell [5] considered a number of variables to control the quality of SLM printed parts. Their work focused on the scanning and layer deposition process, concluding that these factors have an effect on the density and surface finish of printed parts. They found optimization of the processing parameters can result in relatively high density parts. K. Saeidi et al. [6] built on studies of process parameter optimization to investigate the solidification process in SLM printed 316L stainless steel. They found the cooling conditions in laser melting were enough to form columnar structures, with sub-grains much smaller than those found in other rapidly cooled manufacturing processes. Scanning transmission electron microscopy (STEM) imaging of the samples indicated the SLM parts had inhomogeneous diffusion in the sub-grain boundaries and chromium silicate nano-inclusions. These features and the high density of the part resulted in high microhardness. Kruth et al. [7] investigated deformation in builds based on powder layer density and scanning strategies, concluding shorter scan length, effective powder coverage and melt of the first layer reduced thermal stresses in the part. This work highlights the impact of factors outside of typical beam scanning machine parameters, but does not proceed to connect the observed effect these factors have on melt and cooling with microstructural observations.

In order to understand SLM as a technology and the structure and performance of the parts it builds, the SLM process and machine factors must be considered as a whole. As the EBM research has shown, there is an impact of factors outside of laser and scanning parameters. This is important to understand as manufacturing of parts on additive systems move towards production of parts of different sizes and build space is optimized. A quantitative understanding of the effects of secondary build variables is necessary for SLM technology. The work presented here intends to address the effects of build location and build part proximity on selectively laser melted 316L stainless steel, through analysis of material structure and properties.

Materials and Methods

The samples for this research were manufactured on a Renishaw AM250, using Renishaw provided 316L stainless steel powder with a particle size distribution of 15-45 µm [13]. The Renishaw AM250 operates a 200W, 1070 nm ytterbium fiber laser with an approximate spot size of 70 µm. The laser scans the build plate and uses point exposures to selectively melt the powder layer, following the computer aided design (CAD) file. These samples were built using 50 micron layers and Renishaw's Meander scanning parameters for 316L. The hatch fill scan parameters are: 200W laser power, a point distance of 50 microns and exposure time of 120 microseconds.

Tensile samples with a radius of 4 mm were built following ASTM E8 [14] in 4 x 4 array or 5 x 5 array as seen in Figure 1. The builds were designed with different spacing between tensile samples, 10, 20, and 40 mm measured from the center of parts, to measure the effect of part proximity. Each build was produced three times for statistical significance. An additional 3 x 3 array was created with a 64 mm part spacing, wherein each part consisted of 5 tensile specimen

stacked in the z-direction as seen in Figure 1. This conformation was only built once because of time and material limitations. All tensile samples were tested in accordance to ASTM E8 [14] under room temperature conditions. Modulus of elasticity, 0.2% offset yield strength, tensile strength, and elongation were measured. All machined gage sections followed the ASTM specification for measurement of the test diameter. Crosshead test speeds were controlled uniformly to minimize any impact of rate sensitivity and loading rates were approximately 620 MPa min^{-1}. The test machines and extensometers meet ASTM E4 [15] and ASTM E83 [16] specifications respectively. Microstructural analysis that was completed via a scanning electron microscopy utilized electron backscatter diffraction (EBSD) images to evaluate grain size and misorientation using Orientation Imaging Microscopy™ analysis software.
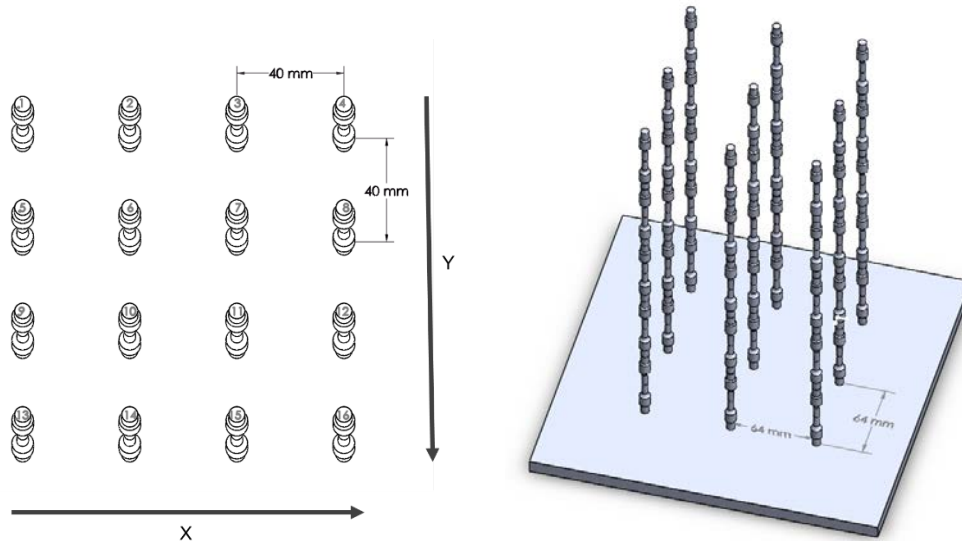

Figure 1: Layout of 40 mm spaced 4x4 array and layout of 3x3 array of 5 stacked tensile bars

Results

The mechanical properties of each sample were measured and analyzed by part location and spacing. The data was analyzed using two different coordinate systems in order to observe possible location based trends. Both coordinate systems were centered on the middle of the build plate. A typical orthogonal coordinate system was used, with x position increasing from left to right, and y position increasing from rear to front as shown in Figure 1. A polar coordinate system, with radial position increasing from the center of the plate outward, and theta position following the standard unit circle was applied as well. The average yield strength, tensile strength, elastic modulus, and elongation were determined for each spacing regime by location. A 95% confidence interval was used on all of the tensile property averages, calculated using two times the standard error of the mean, assuming a normal distribution.

As shown in the ultimate tensile strength results in Figure 2, the 10 and 20 mm spaced parts have an increase in strength across the x axis of the build plate. This is seen to a lesser extent in the 64 mm spaced parts. The yield strength follows the same trend, while the elongation has the

opposite trend. This trend is not seen in the y axis position as presented in Figure 3, where there is no significant change in strength for 10 and 20 mm spaced parts. This follows for yield strength, elongation, and elastic modulus. The x and y axis position for 40 mm spacing shows a slight difference in strength dependent on the distance from the center of the build, which is supported in the radial position graph of tensile strength presented in Figure 4. This trend is not statistically present in any property other than ultimate tensile strength. Additionally, there was no measured effect in any tensile property from z position in the stacked tensile samples as represented by tensile strength shown in Figure 5.
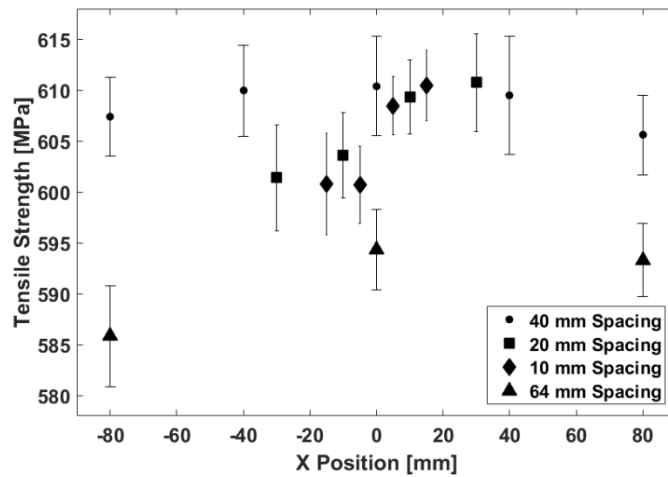
Figure 2: Tensile strength by X axial position for each part spacing with error bars for 95% confidence interval
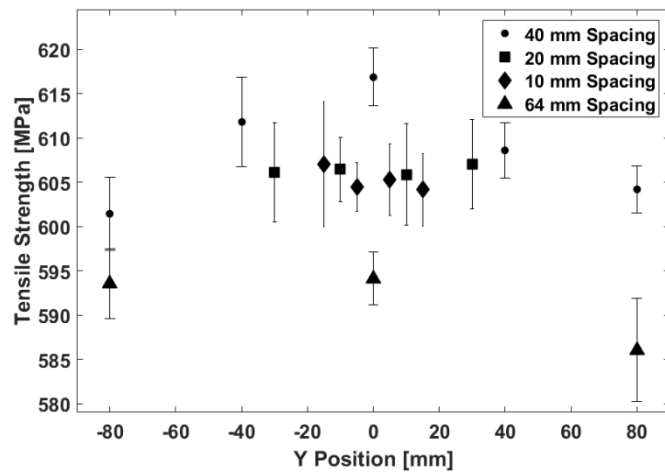

Figure 3: Tensile strength by Y axial position for each part spacing with error bars for 95% confidence interval
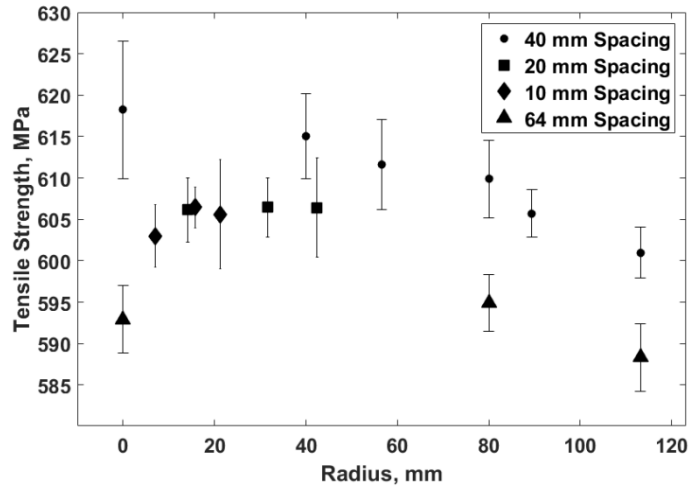
Figure 4: Tensile strength by radial position for each part spacing with error bars for 95% confidence interval
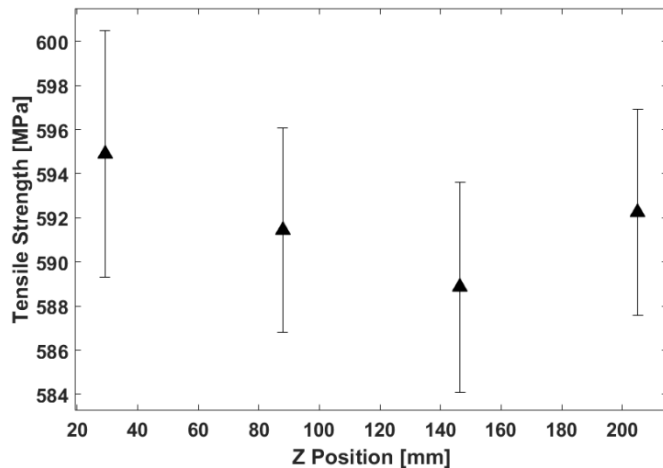
Figure 5: Tensile strength by Z position of 64 mm spaced parts with error bars for 95% confidence interval

Discussion

While the results show trends in the tensile performance based on location factors, it is important to note that this is limited to a small range. The range in ultimate tensile strength was 569-631 MPa, with all the other tensile property ranges being comparably small. The trends observed are statistically significant, but limited to a small range, so in practical applications the difference may not matter.

Analysis of the standard coordinate location scheme showed x position dependence, as exhibited in the 10 mm and 20 mm spaced parts in Figure 2. This was not replicated in the y position analysis, indicating the cause is a unidirectional factor. In the Renishaw AM250, Argon gas flows across the build chamber from positive to negative in the x axis. As the 10 and 20 mm spaced parts saw property changes in the x direction and not in y, it is possible that the strength change is a result of the gas flow. This makes sense as an increase in the temperature or decrease in the velocity of the gas as it flows from right to left would change convection coefficients. As this trend was not exhibited in the parts with greater than 20 mm spacing, the thermal density of

the build may play a role in when gas flow impacts the material properties. Parts built with tighter spacing have more concentrated thermal mass which results in slower cooling from radiation and conduction, allowing for convection to play a larger role and the gas flow to have a greater overall impact.

Decreasing ultimate tensile strength with radial position was only seen in parts with 40 mm spacing, as seen in Figure 4. This trend was not seen in any other tensile property or part spacing. It can be expected that cooling towards the edges of the build volume is faster due to faster conduction outside of the powder bed as those parts are only partially surrounded by the insulating powder bed. A faster cooling rate would most likely be associated with higher dislocation density because as a rapid change in phase is induced, the likelihood of crystallographic flaws due to volume changes is much higher. Additionally, rapid cooling will likely produce small dendritic cells as a result of constitutional undercooling, wherein the number of nucleation sites is increased. Both high dislocation density and small dendritic cells could produce higher strength. The results in this study show lower strength in the regions of predicted faster cooling, the opposite of the expected trend in 40 mm spaced samples.

Due to the lack of a radial trend seen in the 64 mm spaced parts, it appears unlikely that radial location is the single cause of trends seen in the 40 mm spaced samples. While the 64 mm spacing build required significantly more time to build, this increased time is not expected to have significant impact on the properties due to the low operating temperature of approximately 80 C. This conclusion is bolstered by the lack of any trend in tensile properties as a function of build height. Additional causes for this trend in strength could be a difference in density but the density of parts was not seen to trend radially. A second possible cause would be a difference in chemistry between parts in a build.

The chemistry of the parts was analyzed using electron microscopy techniques. The chemistry of parts built with 10 mm, 20 mm and 40 mm spacing indicated no significant difference in composition as described in Table 1. Therefore the differences in tensile properties are not expected to be a result of chemical content differences. The 64 mm spaced parts had higher manganese content, as well as lower sulfur, copper, and vanadium content, which could lead to the slightly lower strength seen in these samples.

Table 1: Average and standard deviation chemical composition by weight percent

	Carbon	Chromium	Manganese	Molybdenum	Nickel	Phosphorus	Sulfur	Silicon
10 mm	0.0262	17.81	1.20	2.344	12.70	0.017	0.010	0.68
	(0.002)	(0.091)	(0.027)	(0.012)	(0.122)	(0.002)	(0.001)	(0.018)
20 mm	0.0263	17.81	1.193	2.344	12.73	0.017	0.010	0.693
	(0.002)	(0.087)	(0.013)	(0.012)	(0.16)	(0.001)	(0.001)	(0.016)
40 mm	0.0238	17.75	1.188	2.337	12.58	0.017	0.010	0.66
	(0.002)	(0.117)	(0.019)	(0.031)	(0.107)	(0.001)	(0.001)	(0.017)
64 mm	0.0263	17.90	1.274	2.369	12.72	0.015	0.007	0.705
	(0.002)	(0.061)	(0.021)	(0.01)	(0.059)	(0.001)	(0.0001)	(0.013)

Optical microscopic images were taken and included in Figure 6. The microstructure samples were etched with an electrolytic 70/30 nitric acid water solution. This is an image of the longitudinal surface of the part, wherein the part was sectioned to expose the XZ face. As Figure 6 shows, optical microscopy shows a dendritic structure, but one cannot clearly delineate grain boundaries from sub-grain solidification structure and therefore optical microscopy was not a suitable method for grain size characterization. Due to this difficulty, EBSD images were taken for microstructural analysis, as large crystallographic misorientation values can be correlated to grain boundaries (Figure 7).
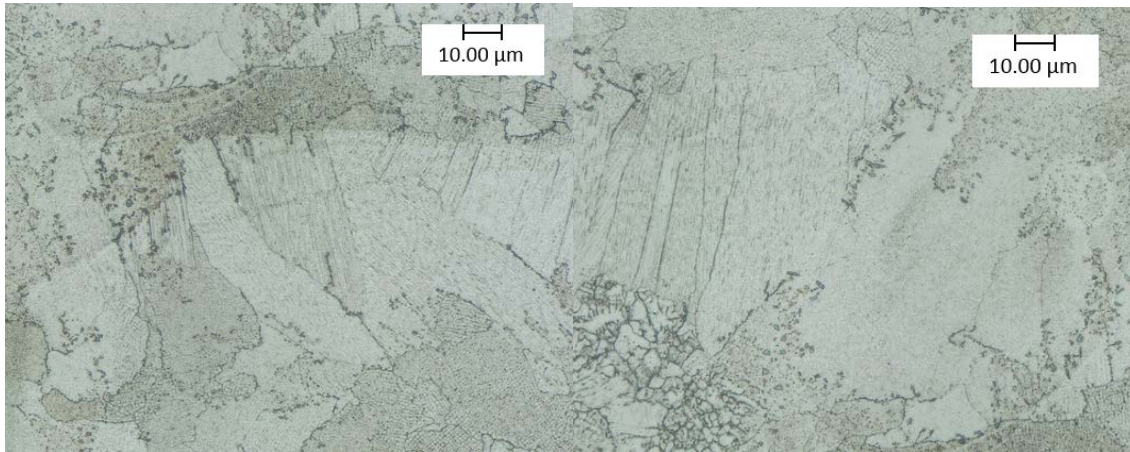
Figure 6: Optical microscope images of 316L longitudinal surface at 2500x, scale on images, etched with an electrolytic nitric solution.
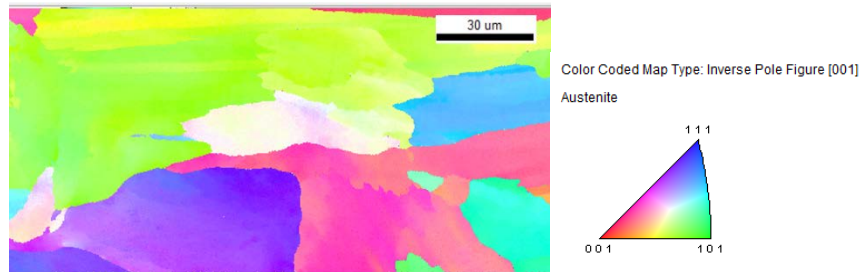

Figure 7: Electron Backscatter Diffraction image of 316L longitudinal surface and inverse pole figure

The EBSD data for all parts showed no ferrite or other inclusions, indicating that all properties are a result of a single phase microstructure. A subset of data was used to evaluate the effect of part location on grain size and yield strength, wherein grain size was reported following ASTM E112 [17]. This subset contained only a few samples from each spacing, therefore statistical analysis could not be effectively performed. From the data collected, individual grains within a single sample ranged in size from less than 10 to over 100 microns. Some of the observed property trends could be caused by grain size as grain boundaries block dislocation motion. The Hall-Petch relationship describes this grain boundary effect, but from the data collected, no such relationship could be determined, as seen in Figure 8. Additionally, no trend between part location and grain size could be determined. The large distribution of grain sizes could explain the difficulties in capturing representative images for analysis. The inability to identify a trend is likely from the small number of data points collected, which limits the likelihood a representative value of the mean grain size is used, and the small number of grains in each EBSD image.
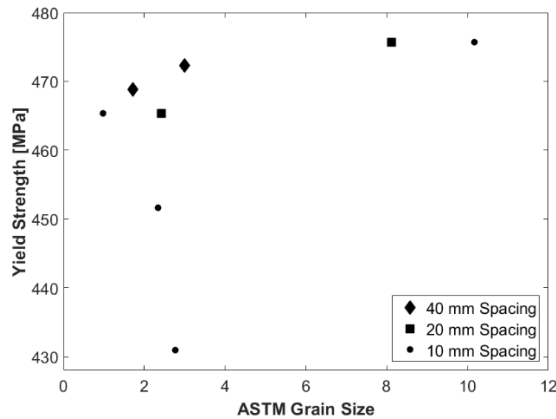
Figure 8: Grain size number versus yield strength of SLM 316L parts printed at different spacing

In addition to grain size, EBSD can provide information on the misorientation within grains which was investigated for potential relationship to part location and effect on material performance. Line scans across several grains in the EBSD images were used to measure the average sub-grain misorientation angle. This misorientation angle represents the difference in the crystallographic orientation within a grain, which can represent dendritic cell structures and the dislocation density within a grain. Again, a subset of data was analyzed and did not show a trend based on part position in build, as seen in Figure 9 for X position. The spread of data based on position shows no dependence in the X, Y or radial position nor part spacing, but the number of data points and lack of statistical significance means this data may not be representative of the populations mean. Additionally, there was no trend between misorientation and yield strength. The data supports relative uniformity in sub-grain misorientation, as the data is mostly limited to a tenth of degree difference. If this is the case, sub-grain strengthening would not explain the differences in tensile strength between spaced parts or the technique used here to represent sub-grain strengthening is not effective.
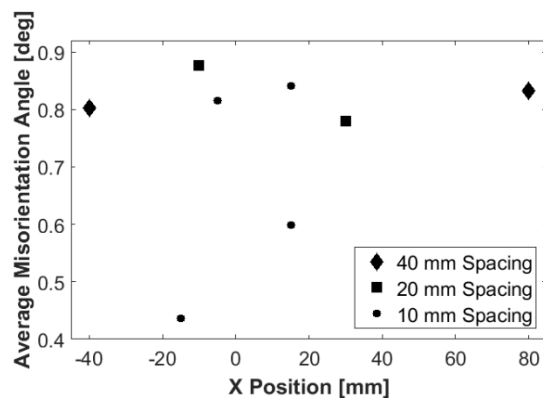

Figure 9: Average sub-grain misorientation angle versus X position of SLM 316L parts printed at different spacing

Conclusions

A study on SLM 316L stainless steel was completed to measure the effect that part location and part spacing has on tensile properties. The data showed there were statistically significant trends based on part location and spacing, but the range in property trends was very small, wherein

there may be no practical, practical difference in performance. The range in ultimate tensile strength was 569-631 MPa, with all the other tensile property ranges being comparably small. It was determined that an effect of the spacing between parts in a build had an effect on tensile properties if the spacing was large enough, but below 40 mm there was no significant difference in performance. Part location was determined to have an effect related to cover gas flow for parts built at 10, and 20 mm spacing, but there was a different radial dependence in the ultimate tensile strength of 40 mm parts. No effect was seen in the tensile properties of parts at different build heights. Preliminary analysis of chemistry, grain size and sub-grain misorientation did not provide additional support for these trends. Additional analysis is needed regarding grain size and sub-grain structure in order to provide greater statistical support for the structure and property relationships seen here. Fractography will also be done to understand the cause of failure the parts and if these are related to location.

Acknowledgments

Conflict of Interest: The authors declare that they have no conflict of interest.

Bibliography

[1] N. Hrabe and T. Quinn. "Effects of processing on microstructure and mechanical properties of a titanium alloy (Ti-6Al-4V) fabricated using electron beam melting (EBM), part 1: Distance from build plate and part size." *Materials Science & Engineering A*, 573 (2013): 264-270.
[2] N. Hrabe and T. Quinn. "Effects of processing on microstructure and mechanical properties of a titanium alloy (Ti-6Al-4V) fabricated using electron beam melting (EBM), part 1: Energy input, orientation, and location," *Materials Science & Engineering A*, 573 (2013): 271-277.
[3] X. Tan et al. "Graded microstructure and mechanical properties of additive manufactured Ti–6Al–4V via electron beam melting," *Acta Materialia,* 97 (2015): 1-16.

[4] S.L. Lu et al. "Microstructure and Mechanical Properties of Long Ti-6Al-4V Robs Additively Manufactured by Selective Electron Beam Melting Out of a Deep Powder Bed and the Effect of Subsequent Hot Isostatic Pressing," *Metallurgical and Materials Transactions A*, 46A (2015): 3824-3834.

[5] K. Adb-Elghany and D. L. Bourell. "Property evaluation of 304L stainless steel fabricated by selective laser melting," *Rapid Prototyping Journal* 18 (2012): 420-430.

[6] K. Saeidi et al. "Hardened austenite steel with columnar sub-grain structure formed be laser melting," *Materials Science and Engineering* A 625 (2015): 221-229.

[7] J.P. Kruth, et al. "Selective laser melting of iron-based powder," *Journal of Materials Processing Technology*, 149 (2004): 616-622.

[8] P.Y. Peretyagin, et al. "Track Geometry in Selective Laser Melting," *Russian Engineering Research,* 35 (2015): 473-476.

[9] B. Song et al, "Differences in microstructure and properties between selective laser melting and traditional manufacturing for fabrication of metal parts: a review," *Mechanical Engineering*, 10 (2015): 111-125.

[10] A.S. Wu et al. "An Experimental Investigation into Additive Manufacturing Induced Residual Stresses in 316L Stainless Steel," *Metallurgical and Materials Transactions A*, 45 A (2014): 6260-6270.

[11] H . K. Rafi, N. V. Karthik et al. "Microstructures and Mechanical Properties of Ti6Al4V Parts Fabricated by Selective Laser Melting and Electron Beam Melting," *Journal of Materials Engineering and Performance*, 22 (2013): 3872-3884.

[12] L. Ladani. "Local and Global Mechanical Behavior and Microstructure of Ti6Al4V Parts Built Using Electron Beam Melting Technology," *Metallurgical and Materials Transactions A*, 46(9) (2015): 3835-3841.

[13] Renishaw, 2015, "SS 316L-0407 powder for additive manufacturing," Renishaw plc, Stone, Staffordshire, UK, 2015. H-5800-3001-01-D, www.renishaw.com/additive.

[14] ASTM Standard E8, 2015, "15a Standard Test Methods for Tension Testing of Metallic Materials," ASTM International, West Conshohocken, PA, 2015, DOI: 10.1520/E0008-15A, www.astm.org.

[15] ASTM Standard E4, 2014 "Standard Practices for Force Verification of Testing Machines," ASTM International, West Conshohocken, PA, 2014, DOI: 10.1520/E0004-14, www.astm.org.

[16] ASTM Standard E83, 2010, "Standard Practice for Verfitication and Clasfficiation of Extensometer Systems," ASTM International, West Conshohocken, PA, 2010, DOI: 10.1520/E0083-10A, www.astm.org.

[17] ASTM Standard E112, 2014, "Standards Test Methods for Determining Average Grain Size," ASTM International, West Conshohocken, PA, 2014, DOI: 10.1520/E0112-13., www.astm.org.